Available online at www.sciencedirect.com
SCIENCE DIRECT®
Journal of Power Sources 146 (2005) 39–44
JOURNAL OF POWER SOURCES
www.elsevier.com/locate/jpowsour

Performance of $LiNiCoO_2$ materials for advanced lithium-ion batteries

Yuichi Itou, Yoshio Ukyo *

Toyota Central R&D Labs Inc., Nagakute, Aichi 480-1192, Japan

Available online 8 August 2005

Abstract

The mechanism of the increasing of resistance of lithium-ion batteries using $Li(Ni,Co)O_2$ based material as positive electrode materials was investigated. The increase in resistance of cells with $Li(Ni,Co)O_2$ material and artificial graphite was observed in cycling test at 60 °C. It was found that the increasing of resistance was mainly attributed to that at positive electrode by 'reconstructed method'. In order to examine the mechanism of the increasing of resistance of positive electrode, the morphological changes of positive particles and local structure of $Li(Ni,Co)O_2$ material were investigated. The clearance and crack were observed at grain boundary inside particle after cycle by FIB (focused ion beam) technique. The change of local structure around Co-atom was observed during charge–discharge process at 60 °C by in situ XAFS (X-ray absorption fine structure spectroscopic) analysis method. It was considered that the morphological and local structural changes of positive material cause the increasing of resistance.

Keywords: Lithium-ion battery; Cycle performance; Deterioration; Focused ion beam; XAFS

1. Introduction

Li–Ni-based material such as $Li(Ni,Co)O_2$ is one of the most promising candidates for a cathode material of advanced lithium-ion battery because of its lower cost and higher capacity compared with $LiCoO_2$ widely used for commercial lithium-rechargeable batteries [1]. The performance of $Li(Ni,Co)O_2$ materials has been studied by many authors [2,3]. For automobile-use, the performance of durability is specially required in the various performances. However, the durable performance of batteries using $Li(Ni,Co)O_2$ based material at high temperature is not clear in detail.

In this study, the deterioration mechanism of lithium-ion batteries using commercial $LiNi_{0.8}Co_{0.15}Al_{0.05}O_2$ as the positive electrode materials was investigated. The cycle performance was examined by 18650-type cell with $LiNi_{0.8}Co_{0.15}Al_{0.05}O_2$ and graphite as positive and negative at 60 °C. The increase in resistance was determined after cycle tests. Firstly, we tried to determine the place in the cell where the resistance increases by 'reconstructed method'. In order to investigate the mechanism of deterioration, morphology changes of positive particles were observed by focused ion beam (FIB) technique. Further more; a change of local structure and electronic state of positive material were analyzed by in situ X-ray absorption fine-structure spectroscopic (XAFS) analysis. On the basis of these results, the mechanism of deterioration will be discussed in this paper.

2. Experimental

2.1. 18650 cells and cycle test condition

18650 cell had a spirally wound electrode. Fig. 1 shows a schematic illustration of 18650 cell. Positive and negative electrode consisted of Al and Cu thin films (current collector) of which both sides were coated by electrode mixture (active materials, conductive carbon and binder). The separator was a micro-porous polyethylene membrane and the electrolyte was EC:DEC with 1 M $LiPF_6$. The chemical composition given by the supplier was $LiNi_{0.8}Co_{0.15}Al_{0.05}O_2$. The cathode was 85% (in weight) active material, 10% conductive material and 5% PVDF binder. The anode was 95% artificial graphite and 5% PVDF binder. The 18650 cells were firstly cycled under constant current at a 0.05 mA cm^{-2} density (discharge) between 4.1 and 3.0 V at 20 °C. This corresponds to

* Corresponding author.

0378-7753/$ – see front matter © 2005 Published by Elsevier B.V.
doi:10.1016/j.jpowsour.2005.03.091

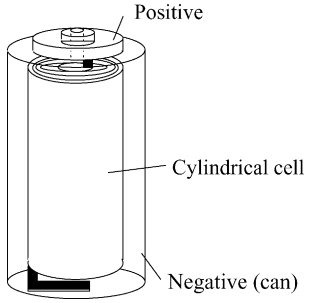

Fig. 1. Schematic illustration of 18650-cell.

a 0.1C rate. The cell was charged from its initial open circuit condition to 4.1 V. The positive delivered 185 mAh g^{-1} capacity during its first charge, and the first discharge of 155 mAh g^{-1}. Resistance is calculated from the change in electric potential when direct current is supplied to the cell for 10 s at 20 °C.

The cycle tests were carried out by constant current density, 2 mA cm^{-2}, between 4.1 and 3.0 V at 60 and 20 °C. This current density corresponds to 2C rate. The capacity and the resistance of the cells after 500 cycles were measured on the same condition, and compared with the initial value.

2.1.1. Determination of the place where the resistance increases

In order to determine the place where resistance increases in the cell, cells were re-constructed with the electrodes after cycles and the new electrodes. The cell after cycle was disassembled under an argon atmosphere, and re-constructed with new electrode under dry air atmosphere. The resistance of the cells with the positive electrode after cycles and the new negative electrode are compared with that of the cell with the new positive and the negative electrode after cycles. This method is named as 'reconstruction method' in this study.

Resistances of positive and negative electrodes are determined separately from total resistance by using Li-metal as reference electrode. This method is named as 'three electrodes method'.

2.1.2. Observation of positive electrode by FIB

In order to investigate the deterioration mechanism, the morphology changes of $LiNi_{0.8}Co_{0.15}Al_{0.05}O_2$ particles were observed by focused ion beam (FIB) technique. The cross-section of electrode was cut smoothly by irradiating of Ga-ion beam, and the surfaces were observed by SEM.

2.2. Cells for in situ XAFS analysis

X-ray absorption fine-structure spectroscopic (XAFS) data for $LiNi_{0.85}Co_{0.15}Al_{0.05}O_2$ (the anode is graphite) were collected at various voltages by using the in situ coin cell newly developed in our laboratory for XAFS measurement. Ni and Co K-edge XAFS data were collected using beam line, No. BL16B2, in SPring 8 [4]. Fig. 2 shows the newly developed coin cell for in situ XAFS measurement. This is the coin cell with Be-windows, which was easy to penetrate by X-rays. The XAFS spectra were measured during charge–discharge process at 20 and 60 °C. Electronic state of Ni and Co ions and, local structural change of positive material were analyzed by measuring XAFS spectra during charge–discharge process.

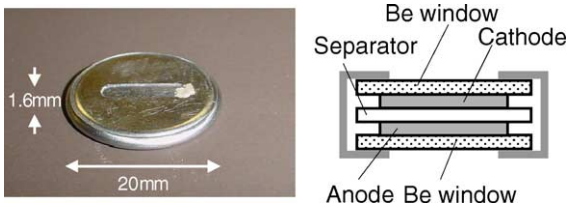

Fig. 2. Schematic illustration of coin-cell.

3. Results and discussion

3.1. Cycle performance

The cycle performance was shown in Fig. 3. Initially discharge capacity was 120 mAh g^{-1}at 20 °C, and no capacity fading was observed even after 500 cycles. On the other hand, initial discharge capacity was 155 mAh g^{-1} at 60 °C, and capacity retention after 500 cycles was very good about 85% of initial capacity. The capacity and the resistance of the cells after 500 cycles were compared with those before cycle test. The results were shown in Fig. 4. Fig. 4(a) shows the capacity and resistance before and after 500 cycles at 20 °C, and Fig. 4(b) shows those at 60 °C. Only small change in capacity and resistance was observed after 500 cycles at 20 °C. At 60 °C, good capacity retention was obtained (10% capacity fading). However, serious increase of resistance was recognized. The resistance before and after cycle test are 80 and 205 mΩ, respectively. The resistance after cycles was 2.5 times higher than that before cycles. It is considered that the increasing in resistance is serious problem than a capacity fading. Therefore, the mechanism of increasing was mainly investigated in the following.

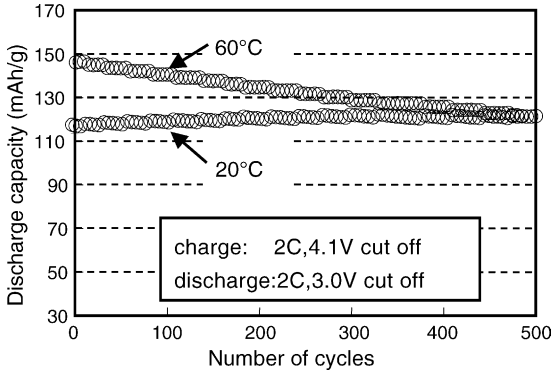

Fig. 3. Cycle performance of 18650-cell at 60 and 20 °C.

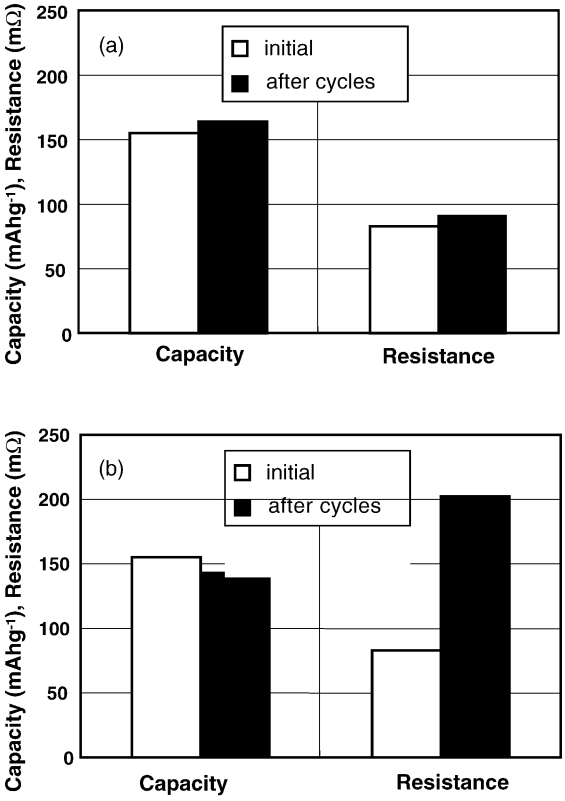

Fig. 4. Capacity and resistance at 20 °C before and after cycles: (a) at 20 °C and (b) at 60 °C.

3.2. Determination of place where resistance increases

It is necessary to determine the place where resistance increases in order to investigate the mechanism of deterioration. The 'reconstruction method' as mentioned in previous chapter was used for this purpose. The result was shown in Fig. 5. The resistance of the cell with the positive after cycles and the new negative are higher than that of the cell with the new positive and the negative electrode after cycles.

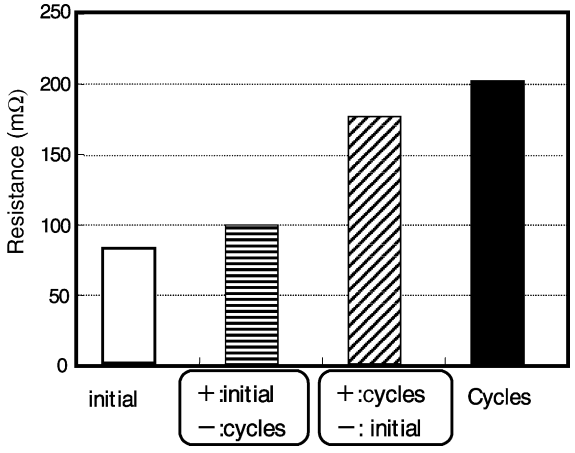

Fig. 5. Resistance of reconstruction cells.

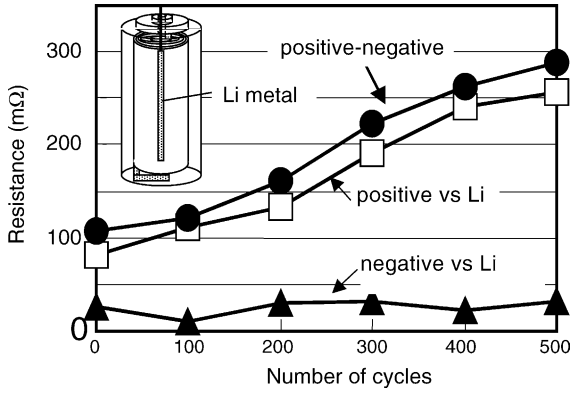

Fig. 6. Change in resistance of three-electrode method during cycles.

This result suggests that the increasing of the resistance were mainly attributed to that of the positive electrode.

Fig. 6 shows changes in the resistance between (1) positive and negative electrodes, (2) positive and reference electrodes, and (3) negative and reference electrodes, during cycle test determined by using 'three electrode method'. While the resistance between positive and negative electrodes are gradually increasing with cycle, the resistance between positive and reference electrodes was increased drastically. On the other hand, the resistance between negative and reference electrodes was almost constant.

This result suggests that the increasing of the resistance were mainly attributed to that of the positive electrode.

The same results were obtained by using two methods.

3.3. Observation of positive electrode by FIB

In order to investigate the detail, the morphology changes of positive particles were observed by FIB (focused ion beam) technique. Fig. 7 shows microscopic images of positive particles on the cross-section of electrode. In Fig. 7(a)–(c) shows the initial state, the states after 500 and 800 cycles. The aggregated particle consists of the some primary particles as shown in Fig. 7(a). The primary particles seem strongly to be connected each other at initial state. However, the clearance and cracks were observed at grain boundary after 500 cycles, and the particles were pulverized after 800 cycles. In order to examine in detail, a change in lattice distortion during charge process was measured by X-ray diffraction method, and morphology changes of particles were observed during charge process. The results were shown in Fig. 8. Fig. 8 shows the change of volume and *c*/*a* ratio during charge process. Fig. 9(a) shows the microscopic image of the particle at $x = 0.08$ in $Li_{1-x}Ni_{0.8}Co_{0.15}Al_{0.05}O_2$ and Fig. 9(b) shows that at $x = 0.6$. During charge, the crystal lattice was distorted, and many cracks and clearance were formed at the grain boundaries.

The mechanism of deterioration was estimated from these results as follows: At initial state of cycle, the morphological change was reversible during charge–discharge, although the crystal lattice was distorted. However, it was considered

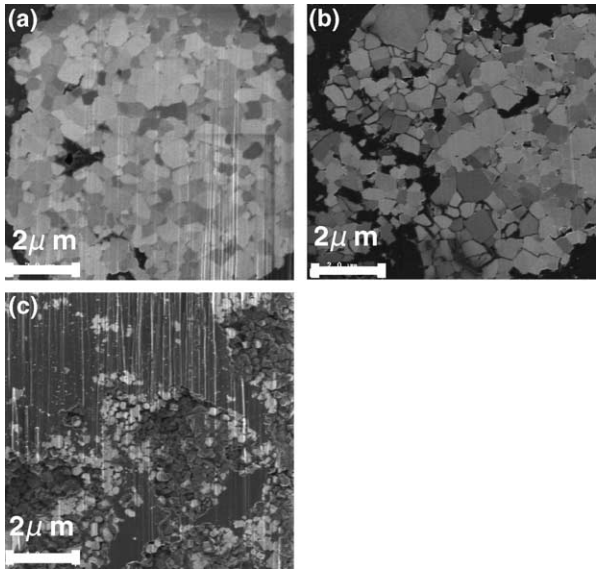

Fig. 7. Morphology of positive particle: (a) before cycle, (b) after 500 cycles and (c) after 800 cycles.

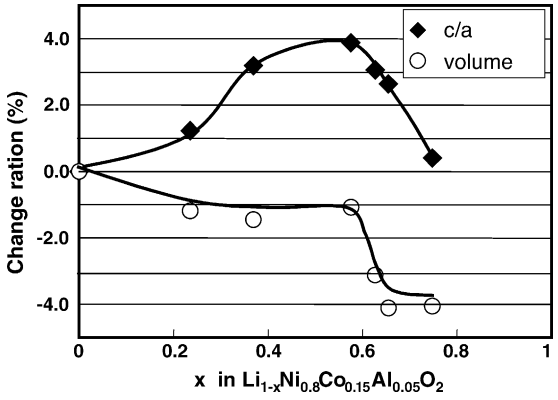

Fig. 8. Change in lattice constant and volume of positive material during charging.

that the morphological change becomes to be irreversible gradually with cycle. Therefore, the clearance and cracks are formed in particles with cycle. It was thought that the resistance at positive electrode increased by declining of electronic conduction, due to the formation of cracks. In order to verify this mechanism, the relation between the increas-

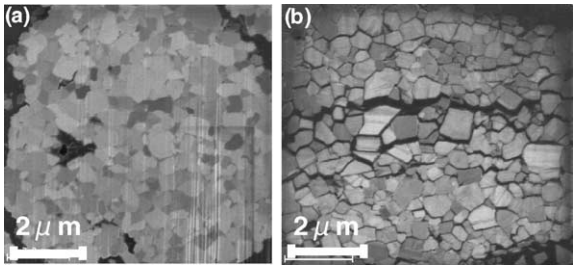

Fig. 9. Morphology of positive particle: (a) state of discharge, (b) state of charge.

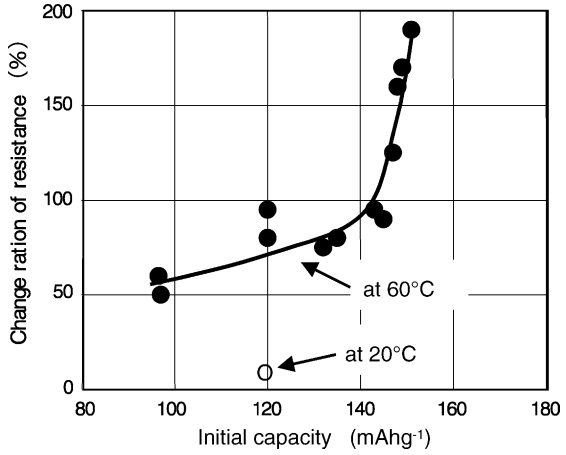

Fig. 10. Relation between change ratio and capacity.

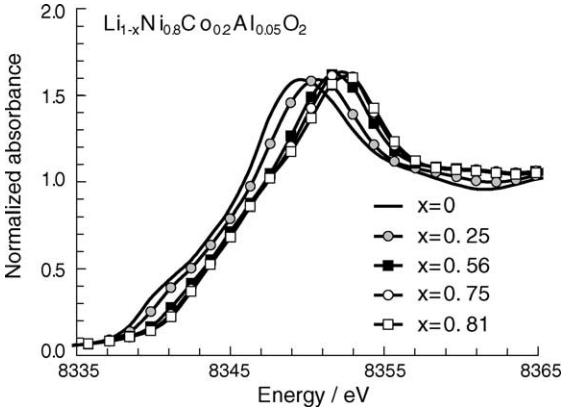

Fig. 11. Ni K-edge XANES spectra at various states.

ing of resistance and potential window during cycling was examined. The result was shown in Fig. 10 which shows the relation between the initial discharge capacity at 60 °C and the increase in resistance. For example, the capacities were 147 mAh g^{-1} between 4.1 and 3.0 V, 98 mAh g^{-1} between 4.1 and 3.5 V and 154 mAh g^{-1} between 4.1 and 2.5 V. The increase in resistance was reduced with decreasing of capac-

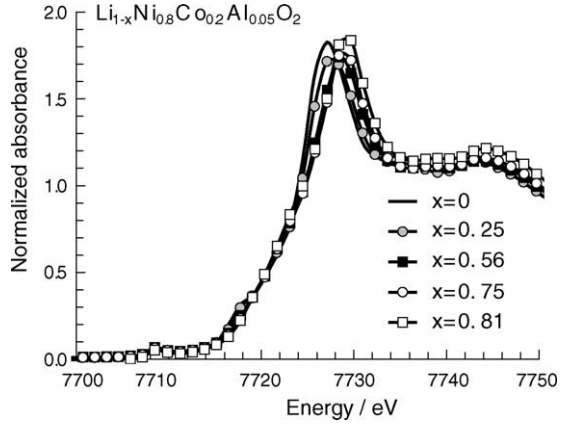

Fig. 12. Co K-edge XANES spectra at various states.

ity or of potential window. This result indicates volume change causes the increase in resistance.

The relation between the increase in resistance after 500 cycles at 20 °C and the initial capacity was plotted in Fig. 10. The increase of resistance at 20 °C is smaller than that at 60 °C. After cycle test at room temperature, small amount of cracks were observed. Therefore, although it is not doubtful that occurrence of crack was one factor of increase in resistance, other factor was also must be taken into consideration.

From this purpose, a change of local structure and an electronic state of positive particle during charge–discharge at 20 °C and 60 °C were analyzed by in situ XAFS analysis method.

3.4. In situ XAFS analysis of positive material

The Ni and Co K-edge XANES spectra at various states before cycling are shown in Figs. 11 and 12. The chemical shifts of the edge peak energy upon charging were found in both edges. Especially, the Ni scans show a steady progress of the entire pattern from lower to higher energy as a function of decreased Li content, indicating an increasing average Ni oxidation. The Fourier-transforms of Ni K-EXAFS spectra at various states of charge before cycling are shown in Fig. 13(a) and (b). The profile of Ni–O peak around 1.5 Å indicates the symmetry of NiO_6 octahedron. The amplitude of this peak increases with the degree of charge. This is due

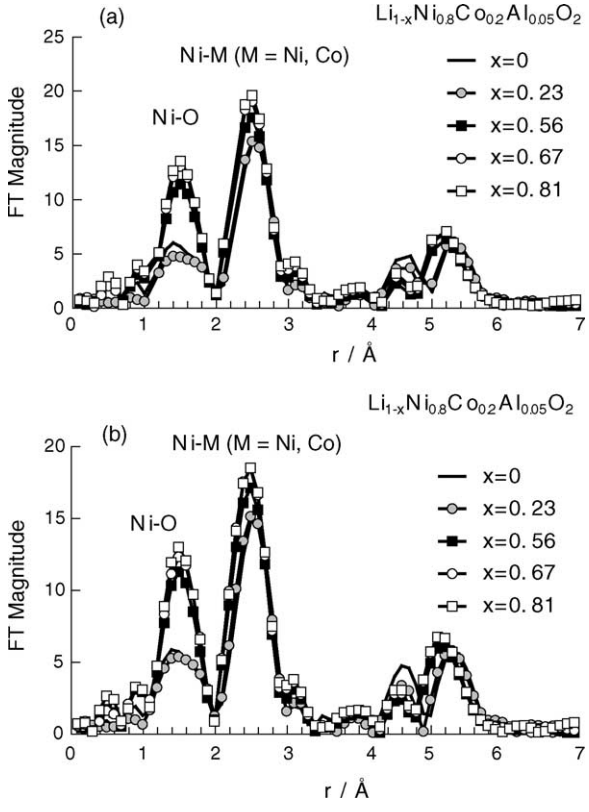

Fig. 13. Fourier-transforms of Ni K-EXAFS spectra at various states during charging: (a) at 20 °C and (b) at 60 °C.

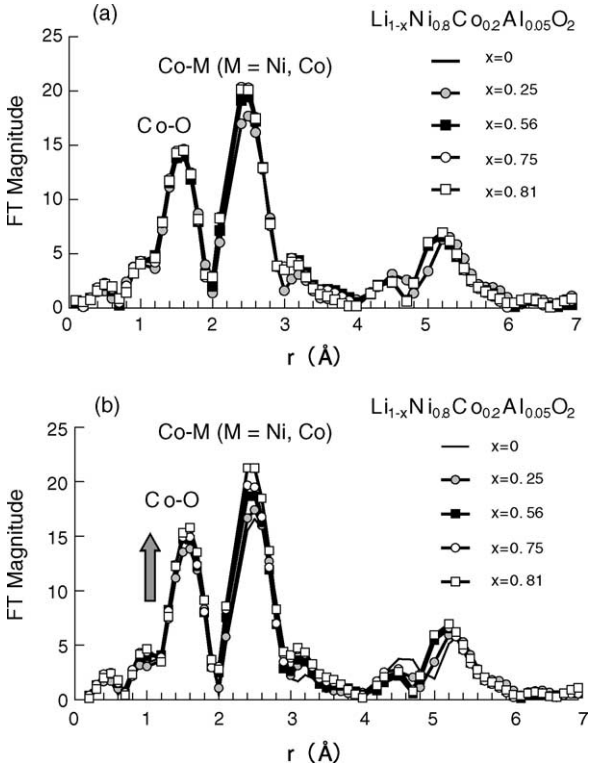

Fig. 14. Fourier-transforms of Co K-EXAFS spectra at various states during charging: (a) at 20 °C and (b) at 60 °C.

to a Jahn-Teller distortion for Ni^{3+}. When Ni is oxidized to Ni^{4+} during charge, the oxygen coordination around the Ni becomes symmetrical and the peak magnitude increases. There is no different between the changes of EXAFS profile during charging at 20 °C and those at 60 °C. Fig. 14(a) and (b) shows Fourier transforms of the Co K-EXAFS spectra at various states during charging. The profile of Co–O peak around 1.5 Å indicates the symmetry of CoO_6 octahedron. There are very little changes in the magnitude of the Co–O peak at 20 °C. This result indicated that the symmetry of CoO_6 octahedron, that is, Debye–Waller factor, hardly changes at 20 °C even if a Jahn–Teller distortion for Ni-ion is released during charging. On the other hand, a change was recognized in the magnitude of the Co–O peak at 60 °C during charge. This result was indicated that the symmetry of CoO_6 octahedron, that is, Debye–Waller factor, changes easily at 60 °C although that hardly changes at 20 °C. It was suggested that the local structural changes of positive material during charge–discharge cause the deterioration at high temperature. The relation between deterioration and the local structural changes of positive material will be examined in detail in future.

4. Conclusion

The mechanism of deterioration of lithium ion batteries using Li–Ni-based material as positive materials was investigated. The following results were obtained.

(1) The large increase in cells resistance with $LiNi_{0.8}Co_{0.15}Al_{0.05}O_2$ and graphite was observed during cycle test at 60 °C in spite of the small capacity fading.
(2) In order to determine the place where the resistance increases, cell were re-constructed with the electrodes after cycles and the new electrodes. The results indicate that the increase in resistance of cell was mainly attributed to the increase in resistance of the positive electrode.
(3) Many cracks were observed at grain boundary in positive particles after cycle by FIB technique.
(4) The local structure and the electronic structure were analyzed by in situ XAFS analysis method. The change of local structure around Co-atom was recognized at 60 °C during charge–discharge process although those changes were not recognized at 20 °C.
(5) It was considered that the increase of resistance was caused by the morphological change of particles and local structural changes of positive material.

Acknowledgments

The authors express their thanks to members of Battery Laboratory (H. Kondo, S. Kawauchi, K. Mukai, T. Sasaki, H. Matsuo, T. Kobayashi, C. Okuda, O. Hiruta and Y. Takeuchi) and Nano-analysis Laboratory (Y. Kondo, T. Nonaka and Y. Seno) in Toyota Central R&D Labs Inc., for discussion and technical support.

References

[1] K. Sekai, H. Azuma, A. Omaru, S. Fujita, J. Power Sources 43 (1993) 241–244.
[2] T. Ohzuk, A. Ueda, M. Nagayama, J. Electrochem. Soc. 140 (1993) 1862–1870.
[3] L. Nakai, K. Takahashi, Y. Shiraishi, T. Nakagome, F. Izumi, Y. Ishii, F. Nishikawa, T. Konishi, J. Power Sources 68 (1997) 536–539.
[4] T. Nonaka, C. Okuda, Y. Ukyo, T. Okamoto, J. Synchrotron Rad. 8 (2001) 869–871.